

Thallium-isotopic compositions of euxinic sediments as a proxy for global manganese-oxide burial

Jeremy D. Owens^{1,2,3*}, Sune G. Nielsen^{1,2}, Tristan J. Horner^{1,4}, Chadlin M. Ostrander^{1,2,5} and Larry C. Peterson⁶

¹NIRVANA laboratories, Woods Hole Oceanographic Institution, Woods Hole, MA, USA

²Department of Geology and Geophysics, Woods Hole Oceanographic Institution, Woods Hole, MA, USA

³Department of Earth, Ocean and Atmospheric Science and National High Magnet Field Laboratory, Florida State University, Tallahassee, FL, USA

⁴Department of Marine Chemistry and Geochemistry, Woods Hole Oceanographic Institution, Woods Hole, MA, USA

⁵School of Earth & Space Exploration, Arizona State University, Tempe, AZ 85287, USA

⁶Rosenstiel School of Marine and Atmospheric Science, University of Miami, Miami, FL, USA

*jdowens@fsu.edu

Keywords: seawater, Toarcian, global redox, anoxia, Tl, reducing

Abstract

Thallium (Tl) isotopes are a new and potentially powerful paleoredox proxy that may track bottom water oxygen conditions based on the global burial flux of manganese oxides. Thallium has a residence time of ~20 thousand years, which is longer than the ocean mixing time, and it has been inferred that modern oxic seawater is conservative with respect to both concentration and isotopes. Marine sources of Tl have nearly identical isotopic values. Therefore, the Tl sinks, adsorption onto manganese oxides and low temperature oceanic crust alteration (the dominant seawater output), are the primary controls of the seawater isotopic composition. For relatively short-term, ~million years, redox events it is reasonable to assume that the dominant mechanism that alters the Tl isotopic composition of seawater is associated with manganese oxide burial because large variability in low temperature ocean crust alteration is controlled by long-term, multi-million years, average ocean crust production rates.

This study presents new Tl isotope data for an open ocean transect in the South Atlantic, and depth transects for two euxinic basins (anoxic and free sulfide in the water column), the Cariaco Basin and Black Sea. The Tl isotopic signature of open ocean seawater in the South Atlantic was found to be homogeneous with $\epsilon^{205}\text{Tl} = -6.0 \pm 0.3$ (± 2 SD, $n = 41$) while oxic waters from Cariaco and the Black Sea are -5.6 and -2.2, respectively. Combined with existing data from the Pacific and Arctic Oceans, our Atlantic data establish the conservatism of Tl isotopes in the global ocean. In contrast, partially- and predominantly-restricted basins reveal Tl isotope differences that vary between open-ocean (-6) and continental material (-2) $\epsilon^{205}\text{Tl}$, scaling with the degree of restriction. Regardless of the differences between basins, Tl is quantitatively removed from their euxinic waters below the chemocline. The burial of Tl in euxinic sediments is estimated to be an order of magnitude less than each of the modern ocean outputs and imparts no isotopic fractionation. Thallium removal into pyrite appears to be associated with a small negative fractionation between -1 and -3 $\epsilon^{205}\text{Tl}$, which renders Tl-depleted waters below the chemocline enriched in isotopically-heavy Tl. Due to the quantitative removal of Tl from euxinic seawater, Tl isotope analyses of the authigenic fraction of underlying euxinic sediments from both the Black Sea and Cariaco Basin capture the Tl isotope value of the oxic portion of their respective water column with no net isotope fractionation. Since the Tl isotope composition of seawater is largely dictated by the relative fraction of Mn-oxide burial versus oceanic crust alteration, we contend that the Tl isotope composition of authigenic Tl in black shales, deposited under euxinic conditions but well-connected to the open ocean, can be utilized to reconstruct the Tl isotope composition of seawater, and thus to reconstruct the global history of Mn-oxide burial.

1. Introduction

The availability of free oxygen in the atmosphere and oceans is thought to be one of the most critical parameters in determining the range and diversity of complex life and ecosystems. More than likely, the surficial evolution of (de-)oxygenation has been the dominant factor for the advancement and restriction of complex life evolution and ecosystems throughout Earth's history including many extinction events in the Phanerozoic. However, directly reconstructing oxygen levels is impossible due to a lack of preservation. Thus, past $[O_2]$ changes must be inferred from proxy evidence that faithfully tracks and records changes in ocean oxygenation. To-date directly tracking the initial changes in global oceanic bottom water (de-)oxygenation has proven to be difficult.

Manganese (Mn) oxides are one of the first minerals to form in the presence of free oxygen at natural seawater conditions based on electron potential (Rue et al., 1997). Thus, the global Mn-oxide flux should therefore be a critical parameter for tracking the expansion or reduction of free oxygen in the global ocean both past and present, making it important to understand and quantify global Mn-oxide burial fluxes today and in the past (e.g., Johnson et al., 2016). However, Mn itself has a short marine residence time (Tribovillard et al., 2006), which prohibits using Mn flux rates from individual sediment cores to reconstruct the global Mn-oxide burial flux. In addition, Mn only has one geologically stable isotope making it impossible to track its mass balance.

Importantly, many redox-sensitive trace metals are strongly sorbed onto Mn-oxides [i.e. V, Ni, Cu, Zn, Mo and Tl (as reviewed in Anbar and Rouxel, 2007; Barling et al., 2001; Goldberg, 1954; Little et al., 2014; Morford and Emerson, 1999; Nielsen and Rehkämper, 2012; Nielsen et al., 2017; Tribovillard et al., 2006; Wang et al., 2016; Wasylenki et al., 2008) to the extent that Mn-oxides account for a substantial percentage of the global marine burial fluxes of these elements (Little et al., 2014; Morford and Emerson, 1999; Rehkämper and Nielsen, 2004). In addition, these elements have relatively long residence times compared to ocean mixing. The sorption of Mo, Tl and Zn to Mn-oxides has been shown to impart a large isotopic fractionation and is a substantial portion of the output flux (Anbar and Rouxel, 2007; Barling et al., 2001; Hein et al., 1997; Maréchal et al., 2000; Rehkämper et al., 2002) thus these isotope systems have the potential to track the global Mn-oxide fluxes.

Thallium isotope ratios obtained from pyrite grains have been proposed as a proxy for understanding the global burial of Mn-oxide minerals (Nielsen et al., 2011b), but the use of Tl isotopes as a tracer of past Mn-oxide burial has not been explored in great detail. To-date, no reliable archive has been identified to reconstruct the Tl isotope composition of seawater

accurately and with sufficient stratigraphic age control to allow detailed paleoceanographic interpretations.

This study aims to expand the utility of Tl isotopes to accurately track Mn-oxide burial by showing that modern organic-rich sediments deposited in euxinic environments capture the Tl isotope composition of the overlying water column with no net isotope fractionation. This clear demonstration opens the door to utilizing black shales deposited throughout Earth history as a direct means of measuring the Tl isotope composition of ancient oceans. In turn, records of seawater Tl isotope compositions offer the promise of information on the history of Mn-oxide burial and, thereby, ocean oxygenation.

2. Thallium isotope background

Several recent reviews have given detailed accounts of the geochemical and isotopic attributes of Tl (Nielsen et al., 2011b; Nielsen et al., 2009; Nielsen et al., 2017); thus, only the salient features of the marine Tl isotopic cycle are described here (Fig. 1). The Tl isotope composition of seawater has been inferred to be homogenous with an average value of $\epsilon^{205}\text{Tl} = -5.8 \pm 0.6$ (2sd) where $\epsilon^{205}\text{Tl} = ((^{205}\text{Tl}/^{203}\text{Tl})_{\text{sample}} - ^{205}\text{Tl}/^{203}\text{Tl}_{\text{NIST 997}}) / (^{205}\text{Tl}/^{203}\text{Tl}_{\text{NIST 997}}) \cdot 10^4$ based on six open ocean seawater analyses from the Arctic and Pacific Oceans. More data are available for Tl concentrations in seawater, which yield an average of 13.3 pg/g or 65 pmol/kg (Flegal and Patterson, 1985). The calculated modern marine residence time of Tl is ~ 18.5 kyr (Baker et al., 2009; Flegal and Patterson, 1985; Nielsen et al., 2017; Rehkämper and Nielsen, 2004).

In the absence of large redox potentials, most environments on Earth have been found to produce limited (Fig. 1) or negligible Tl isotope fractionation (Nielsen and Rehkämper, 2012, and references therein). Therefore, thallium delivered to the ocean by rivers, high-temperature hydrothermal fluids, volcanic sources and mineral aerosols from continental-margin sediments have small variations in the input fluxes (Fig. 1; Nielsen and Rehkämper, 2012, and references therein) but displays near invariant Tl isotope compositions of $\epsilon^{205}\text{Tl} \sim -2$, which is identical to values found for continental crust and melts derived from the upper mantle. Pore waters are the only source that deviates from the -2 input, within analytical error, with values closer to ~ 0 but this likely reflects a small amount of Mn-oxide dissolution.

In contrast, in the modern ocean there are only two known significant oceanic sinks for Tl that impart a fractionation during burial (Fig. 1). These two sinks have been shown to produce large thallium isotope fractionations (Nielsen et al., 2006; Rehkämper et al., 2002; Rehkämper and Nielsen, 2004). Here, we explore Tl isotope systematics during incorporation and burial

of euxinic sediments with Fig. 1 incorporating data discussed in greater detail below. The two output fluxes are [1] scavenging by Mn-oxides and [2] uptake of Tl during low temperature alteration of oceanic crust which represent ~68% and 32% of the burial, respectively. The isotope fractionation associated with Mn-oxides is positive compared to continental crustal material, ϵ^{205} of +6 to +12 with an average of +10, which is likely related to surface oxidation of Tl when sorbed onto the hydrogenous Mn-oxide birnessite (Bidoglio et al., 1993; Nielsen et al., 2013; Peacock and Moon, 2012). This Tl oxidation reaction causes a strong enrichment in ^{205}Tl of almost 20 $\epsilon^{205}\text{Tl}$ -units (Nielsen et al., 2013; Rehkämper et al., 2002). On the other hand, isotope fractionation is likely absent and sorption is weaker for the predominantly high-temperature Mn-oxide todorokite (Peacock and Moon, 2012), which commonly forms at hydrothermal vents. Here we explore the burial of thallium and the isotopic signature in euxinic basins as an additional output flux as it has been suggested that Tl is associated with pyrite burial (Heinrichs et al., 1980; Nielsen et al., 2011b) and the suboxic sink seems to be minimal with $\epsilon^{205}\text{Tl}$ values close 0 (Nielsen et al., 2011b). In addition, there has been a study that suggest enrichments of Tl in surface ocean bacteria (Schedlbauer and Heumann, 2000) and several studies that are suggestive of enhanced burial of Tl in reducing organic rich sediments (Böning et al., 2009; Böning et al., 2017; Borchers et al., 2005) though the isotopic signatures are still unknown. However, a seawater depth transect through a Pacific oxygen minimum zone suggest there is no discernible concentration or isotopic change (Nielsen et al., 2006), the work described here also shows no significant surficial variations to date and the current modern inputs and outputs are well balanced in terms of concentration and isotopes (Nielsen et al., 2017).

Altered oceanic crust is enriched in Tl during circulation of low-temperature (low-T) hydrothermal fluids and exhibits light Tl isotope compositions, with ϵ^{205} values of -6 to -12 with an average isotopic value of ~ -7 , with the shallowest crustal portions characterized by the highest Tl concentrations and lightest isotope compositions (Coggon et al., 2014; Nielsen et al., 2006). The magnitude of global low-T hydrothermal fluid fluxes is controlled by conductive heat loss, which is directly related to the average ocean crust production rate over multi-million-year time scales. Thus, the Tl output flux associated with oceanic crust alteration is not likely changed on short time scales. The mechanism responsible for the incorporation of isotopically light Tl during alteration of oceanic crust is yet to be explained, but could be kinetic in nature (Nielsen and Rehkämper, 2012) and potentially related to partitioning into sulphides (Coggon et al., 2014). Given the invariant nature of Tl isotopes in global Tl input fluxes, these are unlikely to drive significant changes in the Tl isotope composition of seawater (Nielsen et al., 2009). Therefore, the Tl isotope ratio of seawater is controlled almost exclusively by the balance between Mn-oxide burial and low-temperature alteration of oceanic crust (Nielsen et al., 2009).

3. Samples

In this study, we have analysed the Tl isotope composition of seawater samples from four open ocean depth profiles that were collected as part of GA10E/D357 (R/V Discovery; UK GEOTRACES 40°S; Fig. 2). The samples investigated were: Twelve samples from Station 3 (all coordinates are latitude, longitude: -36.46, 13.39 with a depth ranging from 5 m to 3930 m, 11 samples from Station 6 (-39.99, 0.92) ranging from 5 m to 4500 m, 6 samples from Station 8 (-34.31, 17.60) ranging from 29 m to 720 m, and 12 samples from Station 11 (-39.29, 7.65) ranging from 10 m to 5260 m. All GA10E samples were collected using a ‘trace metal-clean’ Ti rosette with PTFE-coated CTD system and deployed using a plasma rope. Samples were filtered through a 0.2 µm filter capsule and transferred into 1L HDPE bottles in a trace metal clean container. Samples were acidified at WHOI (Woods Hole Oceanographic Institution) to pH ~ 2 using concentrated distilled HCl. The water column depth profiles at the four stations intersect numerous water masses including Sub-Antarctic Surface Water, Sub-Tropical Surface Water, Antarctic Intermediate Water, Upper Circumpolar Deep Water, North Atlantic Deep Water and Antarctic Bottom Water (Horner et al., 2015). Precision of seawater Tl isotope measurements was assessed via replicate analyses of SAFe D1, a large-volume sample collected in 2004 at 1,000 m at 30.00 N, 140.00 W during VANC33MV (Johnson et al., 2007).

Cariaco sediment samples were collected in 1990 as part of the PLUME Leg 7 Cruise (R/V Thomas Washington). Six separate box core top samples (0-1 cm) from around the basin including from both sub-basins (Fig. 2) were also collected. All of the Cariaco sediment samples measured in this study were collected below the permanent chemocline (sulfidic portion) at water depths between 410 and 1250 meters. Additional background information and long term data can be found for seawater (Astor et al., 2011) and sediments (Peterson et al., 1990). Seawater samples were collected in 2014 as part of the Carbon Retention In A Colored Ocean (CARIACO) seawater time-series collection. Six samples were collected from this location to capture the first Tl isotope depth profile in the Cariaco Basin from 35 to 400 meters water depth. Water column oxygen concentrations for this particular cruise were not obtained due to instrument issues but there is a wealth of previous data to inform this dataset. The decline in oxygen concentration from many previous sampling campaigns starts at 130 meters depth with a reading of 0 ml/L around 260 to 300 meters depth (Astor et al., 2011). Three samples were obtained in the oxic portion of the water column and three samples from the oxic-anoxic transition or below.

Black Sea sediment samples were collected on the R/V Knorr cruise 134 Leg 8 in 1988 and have since been stored frozen at the WHOI Seafloor Samples Laboratory. Five sub-samples were collected from Station 39 box core 21, which was taken from a water depth of 2092 m (Fig.

2). The box core recovered Unit I, a Holocene finely laminated sapropel (0-25cm), a turbidite layer (25 to 30 cm) and Unit II, a mostly continuous black sapropel. Generally, Unit I contains about 1-5% organic carbon, 10-75% carbonate and the rest constituting detrital clays (Arthur et al., 1994). Unit II generally contains 1-20% organic carbon and 5-15% carbonate (Arthur and Dean, 1998). When subtracting out the turbidite layer, the transition from Holocene laminated sapropel Unit I to Unit II occurs at 25 cm for this core. Seawater samples were collected during Leg 2 of the MedBlack GEOTRACES cruises in 2013 (R/V Pelagia cruise 64PE373). Three samples were analysed at Station 2 at 30 m, 100 m and 150 m. The oxygen concentration at Station 2 starts above 200 $\mu\text{mol/L}$ and declines to 0 $\mu\text{mol/L}$ at ~ 75 m and remains zero to the sediments (Rijkenberg M.J.A., 2013). The distance between the sampling site for sediments and seawater is ~ 82 km.

4. Methods

4.1 Sample preparation and dissolution

Each seawater sample was filtered and acidified at sea using 2.4 ml of 10 M trace-metal grade hydrochloric acid per liter. Additional hydrochloric acid was added to achieve a pH of 0.5 and 10 ml of brominated water was added per liter of seawater prior to column chemistry to oxidize all Tl to the trivalent form. Between 250 and 500 ml of seawater was processed for samples collected from fully oxygenated water, whereas samples taken from below the chemocline in the Cariaco Basin and the Black Sea used ~ 1000 ml to obtain sufficient Tl for a precise isotopic measurement.

Sediments were dried in an oven at 80°C to ensure all remaining water was evaporated. Samples were then powdered using an agate mortar and pestle. The mortar and pestle were cleaned with high purity quartz before each sample and rinsed with deionized water. Bulk samples were dissolved using a two-step procedure to obtain complete dissolution. First, 50-100 mg of samples were reacted with ~ 3 ml of concentrated nitric acid and ~ 3 ml hydrochloric acid and placed in quartz vials in an Anton Paar high pressure asher (HPA) to break all organic molecular bonds below the volatilization temperature of thallium (HPA max of 260°C) and ~ 100 bars of pressure. The samples were then transferred to Teflon vessels and the remaining silicate residues were dissolved using a hydrofluoric/nitric acid mixture. All particulates were completely dissolved prior to anion exchange column chemistry.

Different splits of the same sediment sample and similar weights were also leached using a technique modified from Nielsen et al. (2011b) in order to separate the authigenic component

from the silicate bound Tl. Approximately 50-100 mg of sediment were initially treated with 3 ml of 2 M HNO₃ and heated at 130°C for ~12 hours to chemically separate the authigenic and detrital fraction of Tl. This treatment dissolves pyrite, which is thought to contain the authigenic Tl fraction (Nielsen et al., 2011b), while the undissolved portion is dominated by silicate minerals. The two sample fractions were then separated via three cycles of centrifugation, pipetting off the supernatant (henceforth termed ‘the authigenic fraction’) and rinsing in MQ water. After separation of the authigenic and silicate fractions, both fractions were digested separately in the HPA using ~ 3ml of concentrated nitric and ~3ml of concentrated hydrochloric acid in order to break down organic molecules. After the HPA digestion, authigenic fractions were prepared for anion exchange separation of Tl from the sample matrix; no hydrofluoric acid treatment was used on the authigenic fraction, thereby reducing possible Tl contributions from silicates. Residual silicates were dissolved using a hydrofluoric/nitric acid mixture and then prepared for anion exchange separation (henceforth termed ‘the silicate fraction’).

4.2 Chemical separation and Tl Isotopic Analysis

Thallium purification was done using established ion exchange chromatography protocols (Baker et al., 2009; Nielsen et al., 2004; Rehkämper and Halliday, 1999) and was identical for all samples, seawater and sediments. Briefly, thallium purification was accomplished using two separate columns, one large and one micro-column, using AG1X8 anion exchange resin from Biorad. The two columns quantitatively remove lead (Pb) from the sample, which is required to monitor mass-bias during mass spectrometric analysis. NIST SRM 981 Pb is added to every sample to monitor for instrumental mass bias. In addition, this allows for determination of Tl concentrations during isotopic analysis because the yield of the Tl column chemistry is within error of 100% (Nielsen et al., 2011b; Prytulak et al., 2013).

Following purification, samples were analyzed for Tl isotopic compositions using a Thermo Scientific Neptune multi-collector inductively-coupled-plasma mass-spectrometer (MC-ICP-MS) located in the WHOI Plasma Facility. Thallium isotope analyses utilize standard-sample bracketing as well as external normalization to the added SRM NIST 981 Pb (Baker et al., 2009; Nielsen et al., 2011a; Nielsen et al., 2009; Nielsen et al., 2005; Rehkämper et al., 2002). Thallium isotope compositions are reported relative to NIST SRM 997. The uncertainty of the Tl isotope measurements was assessed specifically during this study via repeat measurements of SAFe D1 seawater sample as well as the USGS shale reference material SCo-1 (Table 1). Eight replicates of SAFe D1 were found to possess a mean $\epsilon^{205}\text{Tl} = -6.0 \pm 0.3$ and Tl concentration of 12.2 ± 2.7 pg/g (60 ± 13 pmol/kg). The authigenic fraction of SCo-1 yielded a

mean Tl-isotope composition of $\epsilon^{205}\text{Tl} = -3.0 \pm 0.2$ and Tl concentration of 214 ± 74 pg/g ($n = 18$) with sample dissolutions and measurements from Woods Hole Oceanographic Institution and Florida State University. The silicate fraction of SCo-1 yielded values of $\epsilon^{205}\text{Tl} = -2.4 \pm 0.4$ and 365 ± 199 ng/g ($n = 12$; all uncertainties are ± 2 SD.) For samples with unknown compositions, we assume that the uncertainty in Tl isotope or Tl concentrations is similar to that obtained for the respective consistency standard (i.e., reproducibility of SAFe D1 applies to other seawater samples, etc.), unless a larger uncertainty was warranted. Overall, our uncertainties are similar to those reported in recent Tl isotope literature (Baker et al., 2009; Coggon et al., 2014; Kersten et al., 2014; Nielsen et al., 2016). Procedural blanks were <5 pg throughout this study, which is insignificant compared to the amounts of Tl processed (>5 ng).

4.3 Pyrite contents

Pyrite sulfur concentrations were obtained on Black Sea sediment samples using a chromium reduction method (Canfield et al., 1986). This method extracts pyritic sulfur using a solution of chromium chloride with hydrochloric acid for two hours, a technique that evolves hydrogen sulfide gas. This gas was precipitated and trapped as silver sulfide (Ag_2S) and quantified using a gravimetric method, which is converted to wt% pyrite-sulfur stoichiometrically.

4.4 Geochemical modeling

A conventional mass balance box model was employed where the ocean is assumed to be a well-mixed reservoir—a reasonable assumption given the relatively long residence times for Mo [~ 450 kyr; (Miller et al., 2011)] and Tl [~ 20 kyr; (Baker et al., 2009; Flegal and Patterson, 1985; Rehkämper and Nielsen, 2004)]. Our model ties the two elemental cycles of Mo and Tl together through the magnitude of global Mn-oxide burial, which represents the ocean reservoir for dissolved metal concentration with fluxes entering and exiting. This follows the approach for many other modeling exercises (Gill et al., 2011; Kump and Arthur, 1999; Reinhard et al., 2013). This time-dependent forward box model (recreating isotopic excursions) was constructed using STELLATM software, and the initial boundary conditions were selected using modern or close to modern values to create a steady-state baseline (Table 2: Anbar and Rouxel, 2007; Nielsen et al., 2017; Reinhard et al., 2013). The steady-state elemental cycles were then perturbed by altering the rate of Mn-oxide burial, which enables a quantitative exploration of the links between the elemental and isotopic cycles of Mo and Tl, as well as their respective perturbation response times. Due to the antithetic isotopic response of Mo and Tl during Mn-oxide burial the

modeling aims to demonstrate the general anti-correlated trends observed in Pearce et al. (2008) and Nielsen et al. (2011b) through the connection of this output parameter. However, our aim is not to directly recreate the data from Pearce et al. (2008) and Nielsen et al. (2011b). Temporal changes in the concentration and isotopic composition of a metal in the ocean can be expressed by the following equation:

$$\frac{\partial M_0^{Me}}{\partial t} = (F_{in1}^{Me} + F_{in2}^{Me} + \dots) - ((F_{out1}^{Me}/M_0^{Me}) + (F_{out2}^{Me}/M_0^{Me}) + \dots) \quad (\text{Eq. 1})$$

is the mass of the dissolved metal in the ocean reservoir. The oceanic inputs (and) delivered to the ocean for Mo are riverine and hydrothermal. The input fluxes for Tl are riverine, hydrothermal, dust aerosols, volcanic emissions and sediment porewaters. The sedimentary outputs (and) for the oceanic molybdenum reservoir are based on the burial redox state and comprise oxic (Mn-oxide burial), reducing (sulfide near the sediment water interface) and euxinic (sulfidic in the water column) conditions. The outputs for the thallium cycle are from Mn-oxide burial termed ‘oxic’ and altered ocean crust. The output fluxes are divided by the mass of the reservoir because the flux of the output is dependent on the size of the current reservoir (Reinhard et al., 2013), which has been shown in the modern ocean for Mo (Algeo and Lyons, 2006). In equations 1 through 3, the terms have been generalized because each elemental cycle has different input and output parameters (see Table 2 for input and outputs).

Combining the isotopic compositions for each parameter in equation 1 allows the simulation of mass and isotopic changes in related reservoirs:

$$\frac{\partial}{\partial t} (M_0^{Me} \delta_0^{Me}) = ((F_{in1}^{Me} \delta_{in1}^{Me}) + (F_{in2}^{Me} \delta_{in2}^{Me}) + \dots) - (((F_{out1}^{Me}/M_0^{Me}) \delta_{out1}^{Me}) + ((F_{out2}^{Me}/M_0^{Me}) \delta_{out2}^{Me}) + \dots) \quad (\text{Eq. 2})$$

In equation 2, represent the Mo and Tl oceanic isotope compositions. Changes in the isotopic composition of Mo and Tl over geologic time are captured in euxinic organic-rich shales (for Mo see Anbar and Rouxel, 2007; for Tl see this study). The isotopic offset between the dissolved metal and incorporation into euxinic sediments is neglected in this model as the fractionation is small for Mo and non-detectable for Tl; thus also describes the isotopic composition of the euxinic output for both cycles. In the model, represents the isotopic composition of the input delivered to the ocean.

Substituting equation 1 into equation 2 and utilizing the product rule, the following expression for the change in the isotopic composition of the ocean over a given time interval can be derived without an assumption of steady-state behavior (following Kump and Arthur, 1999):

$$\frac{\delta_0^{Me}}{dt} = \frac{(F_{in1}^{Me}(\delta_{in1}^{Me} - \delta_0^{Me}) + F_{in2}^{Me}(\delta_{in2}^{Me} - \delta_0^{Me}) + \dots) - ((F_{out1}^{[Me]}/M_0^{[Me]}) (\delta_{out1}^{Me} - \delta_0^{Me})) + (F_{out2}^{[Me]}/M_0^{[Me]}) (\delta_{out2}^{Me} - \delta_0^{Me}) + \dots)}{M_0^{Me}} \quad (\text{Eq. 3})$$

The model tracks isotopic changes in the ocean using archived euxinic sediments. The model is designed to connect the Mo and Tl cycles as they are fractionated in opposite directions

with respect to oxide burial. The Mo and Tl cycles are linked through the global burial of oxic sediments as this is the only output parameter for which both systems have major burial flux and isotopic fractionation. When the output of oxic sediments is perturbed, both elemental cycles are responding to the exact same state change in timing and magnitude, and the values observed are the reservoir and isotopic response. In the model, the Mn-oxide burial flux was increased for 100 thousand years, then returned to the baseline (modern) value, then decreased at the same magnitude as the previous increase for 100 thousand years, and again returned to the baseline value.

5. Results

5.1 Oxic open ocean seawater

The Tl isotope compositions of all 41 samples from the South Atlantic seawater transect exhibit a narrow range from -5.8 to -6.3 (Fig. 3 and Table 3). Taking into account the measurement uncertainty from replicates of SAFe D1 of $\pm 0.3 \text{ } \epsilon^{205}\text{Tl}$ units, the South Atlantic data show no variation within error with an overall average of $\epsilon^{205}\text{Tl} = -6.0 \pm 0.3$ ($n = 41$) and an average concentration of $11.4 \text{ pg/g} \pm 2.1$ or 55.8 pmol/kg ($n = 36$). The seawater data from the SAFe station displays Tl concentrations and isotope compositions identical to the South Atlantic samples as well as other existing data from the Pacific and Arctic (Nielsen et al., 2006; Rehkämper et al., 2002) and suggests that the sample, as opposed to reported issues of Fe contamination (Cutter, 2013), did not suffer any Tl contamination. These values are identical to published data from the Pacific and Arctic (Nielsen et al., 2006; Rehkämper et al., 2002). When considering only data from the completely oxic stations in this study, the South Atlantic transect and the SAFe station, the overall average Tl isotope composition and concentration of seawater obtained are $\epsilon^{205}\text{Tl} = -6.0 \pm 0.1$ ($n = 49$) and $11.5 \pm 1.1 \text{ pg/g}$ or 56.2 pmol/kg ($n = 41$).

5.2 Euxinic basins

Cariaco seawater samples possess homogenous Tl concentrations ($12.2 \pm 0.2 \text{ pg/g}$ or 60 pmol/kg) in the oxic upper 130 m of the water column followed by a steady decline to 1.4 pg/g (6.8 pmol/kg) at 400m depth (Fig. 4 and Table 4). Only the oxic seawater samples were analyzed for Tl isotopes and were found to display relatively invariant values of $\epsilon^{205}\text{Tl} = -5.5 \pm 0.7$; the average is slightly heavier than open ocean seawater.

Three water samples from the Black Sea displayed similar behavior to the Cariaco Basin with the highest concentration observed in the oxic upper part of the water column (7.2 pg/g or

35.2 pmol/kg), followed by a significant drop to 0.3 pg/g (1.6 pmol/kg) at 150m depth (Fig. 5 and Table 4). The isotope composition of the oxic portion of the Black Sea was found to be $\epsilon^{205}\text{Tl} = -2.2$, which is within uncertainty of all known Tl inputs (Nielsen et al., 2011b; Nielsen et al., 2009; Rehkämper and Nielsen, 2004); samples within and below the chemocline exhibit increasing Tl isotope compositions and decreasing Tl content (Fig. 5).

The authigenic analyses of six core top sediment samples from the Cariaco Basin have an average of $\epsilon^{205}\text{Tl} = -5.4$ [excluding one value, see discussion below (Table 1 and average sediment value shown in Fig. 4)] and a concentration range of 300 to 886 ng/g. The five sediment samples from the Black Sea have an average $\epsilon^{205}\text{Tl} = -2.3$ (Table 1 and Fig. 5) and a concentration range of 119 to 584 ng/g. The silicate fraction for the Cariaco Basin average was $\epsilon^{205}\text{Tl} = -2.8$ (Table 1) and the Black Sea average was $\epsilon^{205}\text{Tl} = -2.0$.

6. Discussion and Synthesis

6.1 Modern oxic open ocean seawater

When comparing this oxic seawater data with the existing Tl isotope data (Nielsen et al., 2006; Rehkämper et al., 2002), and when combined together with results originating from highly disparate regions (e.g., South Atlantic and Pacific) and sampling different water masses (e.g. AABW, NADW, AAIW, PDW in the Pacific), including intersecting an oxygen minimum zone in the Pacific (Nielsen et al., 2006), the results demonstrate that the open ocean is homogenous with respect to Tl isotopes. In addition, although there may exist some Tl concentration variations outside analytical error (Table 3), there is currently no evidence that Tl concentrations vary systematically as a function of any physical parameter in the ocean. Thus, the conclusion is that the concentration profile of Tl in the open ocean is not affected significantly by biological uptake or other interactions with marine particles. Seawater samples close to continents, and thereby close to point sources of Tl input to the ocean, do exhibit Tl isotope variations outside analytical reproducibility (Rehkämper et al., 2002), which may be related to both simple mixing between seawater Tl and different inputs, as well as Tl speciation potentially related to organic ligands and/or interaction with other particles (Nielsen et al., 2005; Turner et al., 2010). However, these effects are relatively minor and do not appear to be translated across large distances within the ocean.

6.2 Euxinic basin systematics

Both euxinic basins investigated display Tl isotope compositions heavier than open ocean seawater. In particular, the Black Sea is essentially characterized by what is likely the riverine input value. This, suggests that the heavier Tl isotope compositions in both the Cariaco Basin and Black Sea basins are due to the amount of basinal restriction, with thus the riverine inputs having a greater effect on the more restricted Black Sea. The fact that the Cariaco Basin is much closer to the open ocean value of $-6 \epsilon^{205}\text{Tl}$ than the Black Sea is expected given its more extensive exchange with open ocean seawater. Importantly, the isotope composition recorded in the Black Sea is more positive than expected based on simple mass balance considerations. The major known inputs to the Black Sea are riverine, precipitation, the Azov Sea and the Bosphorus Strait. It is reasonable to ignore precipitation since it likely contains negligible Tl concentrations. Thus, the riverine water input flux is $\sim 45\%$ (Jaoshvili, 2002) while the Azov (contributes 12%) and Bosphorus Strait (43%) supply the remaining $\sim 55\%$ of water (Jaoshvili, 2002). No data exist for the Tl isotope composition or concentration of these two inputs, but it is reasonable to assume that riverine inputs are similar to the global average riverine value of $\epsilon^{205}\text{Tl} = -2$ and 6.6 pg/g (32 pmol/kg). The Azov and Bosphorus Tl input values are much more difficult to assess and are likely both heavier than open ocean seawater. The Azov Sea could have values closer to continental material and the Bosphorus Strait could be a mixture of Atlantic seawater, riverine input to the Mediterranean Sea but remains unconstrained. However, even if these sources had a combined Tl isotope mass balance compositions near $\epsilon^{205}\text{Tl} \sim -4$, the total Tl budget of the Black Sea would still be lighter than the observed value. There is no realistic Tl output from the Black Sea that is characterized by light Tl isotope compositions, which could explain the heavy Tl isotope composition of the Black Sea. One possible process that may explain the lack of influence on the Black Sea Tl isotope composition from marine sources is rapid removal of Tl from saline input waters when these reach the euxinic Black Sea. This hypothesis, however, should be investigated further – for example, via measurements of Black Sea water and sediments near to the Bosphorus Strait.

It is clear from the present dataset that Tl is efficiently removed from euxinic seawater. Thermodynamic calculations have shown that TlS is not stable at the concentrations of Tl and HS^- present in the Black Sea and Cariaco basins (Nielsen et al., 2011b). This calculation is supported by the fact that Tl isotopes are not perturbed within the Pacific gyre oxygen minimum zone, which suggests that low oxygen concentrations do not alter Tl speciation and concentrations in seawater (Fig. 6). In Nielsen et al. (2011b), Tl isotopes in large pyrite grains and leachates were compared and showed identical values, which suggests that Tl is associated with pyrite (Heinrichs et al., 1980; Large et al., 2014). However, detailed studies are needed to

better constrain the enrichment mechanism. The inference is that Tl partitioning into pyrite that forms in the water column causes the drawdown of Tl in euxinic basins. Thallium is well known to form sulfides due to its pre-disposition for covalent bonding, and early diagenetic sedimentary pyrite has previously been shown to contain elevated concentrations of Tl (Nielsen et al., 2011b). Since Tl deposition in euxinic basins is strongly linked with sulfide precipitation, it is possible to calculate a global Tl flux into euxinic sediments based on the Tl/S ratio of the authigenic fraction in modern euxinic sediments. The authigenic Tl fractions in Cariaco and Black Sea sediments contain 300-900 ng/g (ppb) Tl with an average of ~500 ng/g (used below in calculations), and the Black Sea sediments analyzed here contain on average 0.65 wt% pyrite S, resulting in an average Tl/S ratio for the euxinic burial flux of 1.2×10^{-5} (mol/mol) using the average Black Sea Tl. The current global pyrite S burial flux is $\sim 3.6 \times 10^{11}$ mol/year (Kurtz et al., 2003), and 4.5% (1.6×10^{10} mol/year) of this flux likely occurs into euxinic sediments – dominated by the Black Sea (Neretin et al., 2001). Combining the Tl/S ratio of the Black Sea with the euxinic S burial flux, we obtain an average Tl euxinic burial flux of $\sim 1.9 \times 10^5$ mol/year. This calculated Tl flux in euxinic burial is larger than that inferred for anoxic/suboxic sediments of $\sim 2.5 \times 10^4$ mol/year (Nielsen et al., 2011b). However, the new combined flux of Tl into reduced sediments is substantially smaller than the two major Tl sinks that are both at least an order of magnitude greater at 10^6 mol/year (Table 2). Thallium fluxes into reducing sediments are therefore not significant in the modern ocean but further investigation will be needed to constrain the Tl mass balance during times of widespread and expansive reducing conditions.

In addition to strong Tl drawdown, seawater Tl isotope compositions from the Black Sea also reveal heavier values with decreasing Tl concentration (Fig. 5). These coupled changes were modeled using York Regressions in both closed- and open-system isotope reactor models. A closed system Rayleigh fractionation relationship yields an isotope fractionation factor of $\alpha = 0.99992 \pm 0.00002$ during Tl partitioning into pyrite equivalent to an instantaneous fractionation between dissolved Tl and pyrite of -0.8 ± 0.2 (ϵ). It can also be modeled assuming an open system at steady state with $\alpha = 0.99971 \pm 0.00008$, equivalent to an instantaneous fractionation between dissolved Tl and pyrite of -2.9 ± 0.8 (ϵ). Both values likely represent minimum estimates since neither calculation accounts for vertical diffusion, though the steady-state model is likely a more accurate estimation. In the model, errors on $\epsilon^{205}\text{Tl}$ are 0.33, 0.25, and 0.30 and the errors on [Tl] are 1.3, 0.44, and 0.08 pg/g for the samples from 30, 100, and 150 m, respectively.

Given the very low Tl concentrations observed in both euxinic basins at water depths far above the sediment, it is expected that Tl removal from the water column is largely quantitative, such that the authigenic fraction of euxinic sediments and the oxic portion of the water column

should exhibit Tl isotopic equivalence. Our sediment analyses from the Cariaco Basin (Table 1 and average sediment value shown in Fig. 4) and Black Sea (Fig. 5 and Table 1) confirm this, suggesting that Tl is transferred quantitatively from the oxic part of the water column to the authigenic fraction of the sediment. One sample from the Cariaco Basin exhibits $\epsilon^{205}\text{Tl} = -3.9$, which is significantly heavier than the oxic Cariaco water ($\epsilon^{205}\text{Tl} = -5.5$). This sample possessed the smallest authigenic Tl fraction (40% compared with 60% or more for the other core top samples) and thus the heavier Tl isotope composition may be attributed to slight dissolution of the silicate fraction, which would possess $\epsilon^{205}\text{Tl} \approx -2$.

Comparing Tl isotope compositions for the authigenic fractions with that of residual silicates in the core-top sediments for Cariaco sediments show a large offset ($\sim 2.5 \epsilon^{205}\text{Tl}$ -units) between the two fractions, consistent with the authigenic and detrital fractions (Table 1) being reasonably well separated with the partial dissolution technique. The concentrations in the euxinic core top samples are generally weighted toward the authigenic fraction, which contains $\sim 60\%$ of the bulk Tl except for the one outlying isotopic sample. Calculating the bulk $\epsilon^{205}\text{Tl}$ for all of these samples shows that the bulk values record a mixture of these two end members (Table 1). We therefore conclude that seawater Tl isotope signatures are faithfully recorded in the authigenic fraction of the sediments but that samples with only slight to moderate authigenic Tl enrichments should be interpreted with caution. Additionally, this work shows that the basin needs to be in direct communication with the open ocean, such as Cariaco Basin, to record a global seawater signal. Independent evidence for restriction is important but observing both stratigraphic variability and analyzing several basins, if possible, can alleviate such issues.

6.3 Modeling of seawater Mo and Tl isotopes during the T-OAE

Given that the authigenic portion of euxinic black shales record the Tl isotope composition of the overlying water column, we revisit data from the Toarcian oceanic anoxic event (T-OAE at ~ 183 Ma) as these are the only previously published data for ancient euxinic black shales (Nielsen et al., 2011b). The same sample set has also been investigated for Mo isotopes (Pearce et al., 2008) where it was concluded that cyclical Mo isotope variations throughout the T-OAE recorded systematic expansion and contraction of the global extent of euxinia. The samples and data for Mo and Tl isotopes were collected separately; thus, the relationships discussed here are a broad context as it is difficult to directly compare exact stratigraphic relationships. It should be noted that the relatively low resolution Tl isotope data

precludes a statistically meaningful analysis of the correlation between the two isotope systems, which may either be directly antithetic or document a lead-lag correlation. Nevertheless, we aim to construct a new coupled Mo and Tl isotope model designed as a framework for understanding the linked response in these two isotope systems. Using these previously published data to compare Mo and Tl isotopes is the first study to document a possible antithetic relationship between the isotope systematics (Fig. 7).

There is a debate as to whether the Cleveland Basin, from which the samples that record the antithetic Tl and Mo isotope data come, was so restricted during the T-OAE that open ocean conditions were not recorded in this section (McArthur et al., 2008). This argument is based on the severe depletion of the local seawater trace metal inventory. To investigate the antithetic Mo and Tl isotope stratigraphy further, our new model aims to generally replicate the seawater isotope composition of Mo and Tl to explore the coupled relationship between the two systems and its primary driver. It should be noted that the aim of this model is not to resolve the issue of possible restriction here, but simply to highlight the mechanisms by which Tl and Mo isotopes co-vary and under which circumstances they do not.

The marine isotope mass balances of Tl and Mo show that the only known sink to cause large perturbation to the Mo and Tl isotope composition of seawater in opposite directions is Mn-oxides (Anbar, 2004; Anbar and Rouxel, 2007; Nielsen et al., 2011b; Rehkämper and Nielsen, 2004; Siebert et al., 2003). Hence, in our model we test whether the first-order interpretation of the antithetic Mo and Tl isotope data from T-OAE can be explained by variations in Mn-oxide burial alone. Additional redox factors could affect Mo isotopes but may play a smaller role in the Tl-Mo relationship. The results of the model show that the general direction of the Tl and Mo isotope excursions follows from manipulation of the Mn-oxide flux and, importantly, the model can also recreate the magnitude of the excursions reported in Mo (0.8 ‰) and Tl (6 ε units) isotopes (Nielsen et al., 2011b; Pearce et al., 2008) while varying only Mn-oxide burial flux by ± 50 % of the modern values (Fig. 8a). However, successful model runs that account for both the direction and magnitude of the isotope excursions require that the marine reservoir size for Mo, relative to that of Tl, was substantially smaller during the T-OAE than today. Specifically, the Mo concentration of seawater must be reduced to 21.4 nM or lower (Fig. 8b), which is a factor of five lower than present day (107 nM, Miller et al., 2011), and McArthur et al. (2008) suggest a reduced Mo seawater reservoir for this basin. We do not model changes in the Tl reservoir because the Tl sink into reduced sediments in the modern ocean is relatively small; however, changing the reservoir has a minimal effect on the magnitude of the isotopic excursion and the response time is faster to a perturbation. Although significant expansion of marine euxinia would contribute to diminishing the marine Tl reservoir, the likely concomitant lowering of the

Mn-oxide burial flux would act to expand the marine Tl reservoir. Therefore, the direction and magnitude of the marine Tl reservoir during expansion and contraction of euxinia is not readily predictable.

Our model of Tl and Mo isotopes during the T-OAE does not represent a unique solution to the causes and effects of the Mo and Tl isotope variations in the Cleveland Basin. Interpretations that advocate for strong basinal restriction, for example, could equally explain the observed data simply by invoking periodic influx of open ocean seawater into the restricted Cleveland Basin. It is important to stress that the model presented here merely provides a conceptual framework for interpreting systematic Mo and Tl isotope variations in euxinic black shales under the proviso that the water column at the time of deposition was well connected to the open ocean. However, the model shows that Mo and Tl isotopes have the potential to be a powerful paleoredox tool as Tl can provide independent constraints on the marine oxic burial flux, which in turn can potentially be used to extract information regarding the size of the Mo burial flux into reduced sediments.

7. Conclusions

This study has investigated the cycling of Tl from open ocean seawater, through euxinic basins, and deposited as pyrite in euxinic sediments. Oxic seawater samples from the South Atlantic, Pacific, and Arctic show no variation with any physical parameter in the ocean, with $\epsilon^{205}\text{Tl} = -6.0 \pm 0.7$ [n = 57; includes 8 literature samples from (Nielsen et al., 2006; Rehkämper et al., 2002)]. Hence despite its short oceanic residence time (≈ 20 kyr), Tl can be considered a conservative element in the modern ocean.

Water samples from the euxinic Black Sea and Cariaco Basin show that the concentration of Tl drops dramatically below the chemocline, which is interpreted to reflect Tl partitioning into pyrite that forms in the water column. Importantly, sediments from these two modern euxinic basins faithfully record the $\epsilon^{205}\text{Tl}$ values from the oxic portion of the water column in each basin. The relatively more open ocean Cariaco Basin seawater $\epsilon^{205}\text{Tl}$ values are indistinguishable from open ocean values within analytical error whereas the more restricted Black Sea is characterized by Tl isotope compositions similar to continental runoff, which we attribute to increased basinal restriction in the Black Sea. We conclude that Tl is quantitatively removed from both euxinic basins, and the authigenic Tl isotope signature in the sediments captures the overlying oxic seawater value with no net isotope fractionation. Thus, this work shows that the authigenic fraction of euxinic sediments faithfully record the seawater value. The seawater Tl isotope is

dictated by the magnitude of the two output fluxes while geologically short-term events are likely due to changes in the amount of Mn-oxide burial because shifts in altered oceanic crust burial are on the order of many millions of years. This work documents that Tl isotopes from euxinic basins with limited restriction have the potential to reconstruct Mn-oxide burial; thus, it is important to observe stratigraphic trends and to analyze samples from multiple basins where possible, so that the effects of basin restriction can be evaluated. Studies of Tl isotopes in ancient euxinic black shales have the potential to provide a direct record of the Tl isotope composition of seawater, so long as the sediment depositional environment was well connected to the open ocean.

We use a simple one-box model to show how Tl isotopes can provide previously unavailable constraints on the global burial flux of Mn-oxides, which is a critical parameter for understanding other isotopic and elemental mass balances. Given that many climatic events were likely accompanied by major perturbations in the global Mn-oxide flux, measurement of Tl isotopes in black shales—ideally combined with other isotope systems—promises to reveal unparalleled information regarding the changes in ocean redox over a range of timescales.

Acknowledgements

We would like to thank Jerzy Blusztajn and Paul Caffey at WHOI and Mary Powell and Nevin Kozik at FSU for analytical and instrumental assistance. JDO and SGN would like to thank NSF and NASA for funding; JDO and TJH gratefully acknowledges support from the Agouron Institute Postdoctoral Fellowship Program. This manuscript has benefited from reviews by Tom Algeo, Christian März, an anonymous reviewer and editorial handling from Horst Marschall. Additionally, we would like to thank GA10E/D357 Chief Scientist Gideon Henderson and the GEOTRACES 40°S research crew, in particular Maeve Lohan and Angie Milne, who masterminded filling our bottles; 64PE373 Chief Scientist Micha Rijkenberg and the entire scientific crew on the Black Sea sampling and intercalibration; and the CARIACO time series crew, especially Eric Tappa.

References

- Algeo, T.J., Lyons, T.W., 2006. Mo–total organic carbon covariation in modern anoxic marine environments: Implications for analysis of paleoredox and paleohydrographic conditions. *Paleoceanography*, 21(1): PA1016.
- Anbar, A.D., 2004. Molybdenum Stable Isotopes: Observations, Interpretations and Directions. *Reviews in Mineralogy and Geochemistry*, 55(1): 429–454.

- Anbar, A.D., Rouxel, O., 2007. Metal Stable Isotopes in Paleoceanography. *Annual Review of Earth and Planetary Sciences*, 35(1): 717–746.
- Arthur, M.A., Dean, W.E., 1998. Organic-matter production and preservation and evolution of anoxia in the Holocene Black Sea. *Paleoceanography*, 13(4): 395-411.
- Arthur, M.A. et al., 1994. Varve calibrated records of carbonate and organic carbon accumulation over the last 2000 years in the Black Sea. *Global Biogeochemical Cycles*, 8(2): 195-217.
- Astor, Y.M., Lorenzoni, L., Scranton, M., 2011. Handbook of Methods for the Analysis of Oceanographic Parameters at the Cariaco Time Series Station. Available on line at: <http://www.us-ocb.org/documents/CARIACOMethods.pdf>.
- Baker, R.G.A., Rehkämper, M., Hinkley, T.K., Nielsen, S.G., Toutain, J.P., 2009. Investigation of thallium fluxes from subaerial volcanism—Implications for the present and past mass balance of thallium in the oceans. *Geochimica et Cosmochimica Acta*, 73(20): 6340-6359.
- Barling, J., Arnold, G.L., Anbar, A.D., 2001. Natural mass-dependent variations in the isotopic composition of molybdenum. *Earth and Planetary Science Letters*, 193(3–4): 447–457.
- Bidoglio, G., Gibson, P.N., O’Gorman, M., Roberts, K.J., 1993. X-ray absorption spectroscopy investigation of surface redox transformations of thallium and chromium on colloidal mineral oxides. *Geochimica et Cosmochimica Acta*, 57(10): 2389-2394.
- Böning, P., Brumsack, H.-J., Schnetger, B., Grunwald, M., 2009. Trace element signatures of Chilean upwelling sediments at ~ 36°S. *Marine Geology*, 259(1–4): 112-121.
- Böning, P., Ehlert, C., Niggemann, J., Schnetger, B., Pahnke, K., 2017. Thallium dynamics in the Weser estuary (NW Germany). *Estuarine, Coastal and Shelf Science*, 187: 146-151.
- Borchers, S.L., Schnetger, B., Böning, P., Brumsack, H.J., 2005. Geochemical signatures of the Namibian diatom belt: Perennial upwelling and intermittent anoxia. *Geochemistry, Geophysics, Geosystems*, 6(6): Q06006.
- Canfield, D.E., Raiswell, R., Westrich, J.T., Reaves, C.M., Berner, R.A., 1986. The use of chromium reduction in the analysis of reduced inorganic sulfur in sediments and shales. *Chemical Geology*, 54(1–2): 149–155.
- Coggon, R.M. et al., 2014. Controls on thallium uptake during hydrothermal alteration of the upper ocean crust. *Geochimica et Cosmochimica Acta*, 144: 25-42.
- Cutter, G.A., 2013. Intercalibration in chemical oceanography—Getting the right number. *Limnology and Oceanography: Methods*, 11(7): 418-424.
- Flegal, A.R., Patterson, C.C., 1985. Thallium concentrations in seawater. *Marine Chemistry*, 15(4): 327-331.

- Gill, B.C. et al., 2011. Geochemical evidence for widespread euxinia in the Later Cambrian ocean. *Nature*, 469(7328): 80–83.
- Goldberg, E.D., 1954. Marine Geochemistry 1. Chemical Scavengers of the Sea. *The Journal of Geology*, 62(3): 249-265.
- Hein, J.R. et al., 1997. Iron and manganese oxide mineralization in the Pacific. Geological Society, London, Special Publications, 119(1): 123-138.
- Heinrichs, H., Schulz-Dobrick, B., Wedepohl, K.H., 1980. Terrestrial geochemistry of Cd, Bi, Tl, Pb, Zn and Rb. *Geochimica et Cosmochimica Acta*, 44(10): 1519-1533.
- Horner, T.J., Kinsley, C.W., Nielsen, S.G., 2015. Barium-isotopic fractionation in seawater mediated by barite cycling and oceanic circulation. *Earth and Planetary Science Letters*, 430: 511-522.
- Jaoshvili, S., 2002. The rivers of the Black Sea. 71.
- Johnson, J.E., Webb, S.M., Ma, C., Fischer, W.W., 2016. Manganese mineralogy and diagenesis in the sedimentary rock record. *Geochimica et Cosmochimica Acta*, 173: 210-231.
- Johnson, K.S. et al., 2007. Developing standards for dissolved iron in seawater. *Eos, Transactions American Geophysical Union*, 88(11): 131-132.
- Kersten, M. et al., 2014. Tracing Anthropogenic Thallium in Soil Using Stable Isotope Compositions. *Environmental Science & Technology*, 48(16): 9030-9036.
- Kump, L.R., Arthur, M.A., 1999. Interpreting carbon-isotope excursions; carbonates and organic matter. *Chemical Geology*, 161(1–3): 181–198.
- Kurtz, A.C., Kump, L.R., Arthur, M.A., Zachos, J.C., Paytan, A., 2003. Early Cenozoic decoupling of the global carbon and sulfur cycles. *Paleoceanography*, 18(4): 1090.
- Large, R.R. et al., 2014. Trace element content of sedimentary pyrite as a new proxy for deep-time ocean–atmosphere evolution. *Earth and Planetary Science Letters*, 389: 209-220.
- Little, S.H., Vance, D., Walker-Brown, C., Landing, W.M., 2014. The oceanic mass balance of copper and zinc isotopes, investigated by analysis of their inputs, and outputs to ferromanganese oxide sediments. *Geochimica et Cosmochimica Acta*, 125: 673-693.
- Maréchal, C.N., Nicolas, E., Douchet, C., Albarède, F., 2000. Abundance of zinc isotopes as a marine biogeochemical tracer. *Geochemistry, Geophysics, Geosystems*, 1(5): 1–15.
- McArthur, J.M., Algeo, T.J., van de Schootbrugge, B., Li, Q., Howarth, R.J., 2008. Basinal restriction, black shales, Re-Os dating, and the Early Toarcian (Jurassic) oceanic anoxic event. *Paleoceanography*, 23(4): PA001607.
- Miller, C.A., Peucker-Ehrenbrink, B., Walker, B.D., Marcantonio, F., 2011. Re-assessing the surface cycling of molybdenum and rhenium. *Geochimica et Cosmochimica Acta*, 75(22): 7146–7179.

- Morford, J.L., Emerson, S., 1999. The geochemistry of redox sensitive trace metals in sediments. *Geochimica et Cosmochimica Acta*, 63(1–12): 1735–1750.
- Neretin, L.N., Volkov, I.I., Böttcher, M.E., Grinenko, V.A., 2001. A sulfur budget for the Black Sea anoxic zone. *Deep Sea Research Part I: Oceanographic Research Papers*, 48(12): 2569–2593.
- Nielsen, S., Rehkämper, M., 2012. Thallium Isotopes and Their Application to Problems in Earth and Environmental Science. In: Baskaran, M. (Ed.), *Handbook of Environmental Isotope Geochemistry. Advances in Isotope Geochemistry*. Springer Berlin Heidelberg, pp. 247–269.
- Nielsen, S.G. et al., 2011a. New age for ferromanganese crust 109D-C and implications for isotopic records of lead, neodymium, hafnium, and thallium in the Pliocene Indian Ocean. *Paleoceanography*, 26(2): PA2213.
- Nielsen, S.G. et al., 2011b. Thallium isotopes in early diagenetic pyrite – A paleoredox proxy? *Geochimica et Cosmochimica Acta*, 75(21): 6690–6704.
- Nielsen, S.G. et al., 2009. Thallium isotope evidence for a permanent increase in marine organic carbon export in the early Eocene. *Earth and Planetary Science Letters*, 278(3–4): 297–307.
- Nielsen, S.G., Rehkämper, M., Baker, J., Halliday, A.N., 2004. The precise and accurate determination of thallium isotope compositions and concentrations for water samples by MC-ICPMS. *Chemical Geology*, 204(1–2): 109–124.
- Nielsen, S.G. et al., 2005. Thallium isotope composition of the upper continental crust and rivers: An investigation of the continental sources of dissolved marine thallium. *Geochimica et Cosmochimica Acta*, 69(8): 2007–2019.
- Nielsen, S.G., Rehkämper, M., Prytulak, J., 2017. Investigation and Application of Thallium Isotope Fractionation. *Reviews in Mineralogy & Geochemistry*, 82(1): 759–798.
- Nielsen, S.G. et al., 2006. Hydrothermal fluid fluxes calculated from the isotopic mass balance of thallium in the ocean crust. *Earth and Planetary Science Letters*, 251(1–2): 120–133.
- Nielsen, S.G. et al., 2013. Towards an understanding of thallium isotope fractionation during adsorption to manganese oxides. *Geochimica et Cosmochimica Acta*, 117: 252–265.
- Nielsen, S.G. et al., 2016. Tracking along-arc sediment inputs to the Aleutian arc using thallium isotopes. *Geochimica et Cosmochimica Acta*, 181: 217–237.
- Peacock, C.L., Moon, E.M., 2012. Oxidative scavenging of thallium by birnessite: Explanation for thallium enrichment and stable isotope fractionation in marine ferromanganese precipitates. *Geochimica et Cosmochimica Acta*, 84: 297–313.
- Pearce, C.R., Cohen, A.S., Coe, A.L., Burton, K.W., 2008. Molybdenum isotope evidence for global ocean anoxia coupled with perturbations to the carbon cycle during the Early Jurassic. *Geology*, 36(3): 231–234.

- Peterson, L.C., Overpeck, J.T., Murray, D.W., 1990. A High-Resolution Paleoenvironmental Study of the Cariaco Basin, Venezuela: Late Quaternary to Present - Preliminary Report on R/V Thomas Washington Cruise PLUME-07. RSMAS/University of Miami Technical Report: 50.
- Prytulak, J., Nielsen, S.G., Plank, T., Barker, M., Elliott, T., 2013. Assessing the utility of thallium and thallium isotopes for tracing subduction zone inputs to the Mariana arc. *Chemical Geology*, 345: 139-149.
- Rehkämper, M. et al., 2002. Thallium isotope variations in seawater and hydrogenetic, diagenetic, and hydrothermal ferromanganese deposits. *Earth and Planetary Science Letters*, 197(1–2): 65-81.
- Rehkämper, M., Halliday, A.N., 1999. The precise measurement of Tl isotopic compositions by MC-ICPMS: Application to the analysis of geological materials and meteorites. *Geochimica et Cosmochimica Acta*, 63(6): 935-944.
- Rehkämper, M., Nielsen, S.G., 2004. The mass balance of dissolved thallium in the oceans. *Marine Chemistry*, 85(3–4): 125-139.
- Reinhard, C.T. et al., 2013. Proterozoic ocean redox and biogeochemical stasis. *Proceedings of the National Academy of Sciences*, 110(14): 5357-5362.
- Rijkenberg M.J.A., G., 2013. MedBlack GEOTRACES leg 3 Available on line at: <http://www.geotraces.org/library-88/scientific-publications/cruise-reports/857-ga04-3>.
- Rue, E.L., Smith, G.J., Cutter, G.A., Bruland, K.W., 1997. The response of trace element redox couples to suboxic conditions in the water column. *Deep Sea Research Part I: Oceanographic Research Papers*, 44(1): 113–134.
- Schedlbauer, O.F., Heumann, K.G., 2000. Biomethylation of thallium by bacteria and first determination of biogenic dimethylthallium in the ocean. *Applied Organometallic Chemistry*, 14(6): 330-340.
- Siebert, C., Nägler, T.F., von Blanckenburg, F., Kramers, J.D., 2003. Molybdenum isotope records as a potential new proxy for paleoceanography. *Earth and Planetary Science Letters*, 211(1–2): 159–171.
- Tribovillard, N., Algeo, T.J., Lyons, T., Riboulleau, A., 2006. Trace metals as paleoredox and paleoproductivity proxies: An update. *Chemical Geology*, 232(1–2): 12–32.
- Turner, A., Cabon, A., Glegg, G.A., Fisher, A.S., 2010. Sediment–water interactions of thallium under simulated estuarine conditions. *Geochimica et Cosmochimica Acta*, 74(23): 6779-6787.
- Wang, X. et al., 2016. Sedimentary chromium isotopic compositions across the Cretaceous OAE2 at Demerara Rise Site 1258. *Chemical Geology*, 429: 85-92.

Wasylenki, L.E., Rolfe, B.A., Weeks, C.L., Spiro, T.G., Anbar, A.D., 2008. Experimental investigation of the effects of temperature and ionic strength on Mo isotope fractionation during adsorption to manganese oxides. *Geochimica et Cosmochimica Acta*, 72(24): 5997–6005.

Tables

Sample Name	Map Number	Sample			Water Depth (m)	Pyrite Sulfur Content (wt%)	Authigenic				Silicate				Measured Bulk				Calculated Bulk								
		Depth (m)	Latitude	Longitude			²⁰⁵ Tl (ε)	Data (2*std)	n	Tl (ng/g)	Data (2*std)	n	²⁰⁵ Tl (ε)	Data (2*std)	n	Tl (ng/g)	Data (2*std)	n	²⁰⁵ Tl (ε)	Tl (ng/g)							
Standards																											
USGS SCO-1	-	-	-	-	-	-	-3.0	0.2	18	214	73.9	18	-2.4	0.4	12	365	198.9	12	-2.5	0.33	2	680	86.0	2	-2.6	583	
Black Sea																											
KNR 134 39-BC 21 1-2cm	-	0.015	43.09	32.03	2092	0.62	-2.0	0.5	4	291	-	2	-1.9	0.2	4	168	-	1	-2.2	-	1	375	-	1	-1.9	458	
KNR 134 39 BC 21 2-3cm	-	0.025	43.09	32.03	2092	0.84	-2.2	0.1	2	402	-	2	-2.3	0.2	4	183	-	2	-2.7	-	1	463	-	1	-2.2	584	
KNR 134 39 BC 21 3-4cm	-	0.035	43.09	32.03	2092	0.56	-2.2	0.1	4	353	-	2	-1.8	0.5	4	164	-	2	-2.2	-	1	375	-	1	-2.1	517	
KNR 134 39 BC 21 30-31cm	-	0.305	43.09	32.03	2092	0.54	-2.4	0.1	4	119	-	2	-1.9	0.1	4	416	-	2	-2.4	-	1	379	-	1	-2.0	535	
KNR 134 39 BC 21 48-49cm	-	0.485	43.09	32.03	2092	0.70	-2.8	0.1	3	584	-	2	-2.0	0.2	2	67	-	1	-2.9	-	1	402	-	1	-2.7	651	
Cariaco Basin																											
PL07-22Bx	1	0.01	10.87	65.17	656.00	-	-5.9	0.1	2	886	-	2	-3.0	0.1	2	435	-	2	-	-	-	-	-	-	-	-4.94	1322
PL07-89Bx	2	0.01	10.66	64.86	1342.00	-	-3.9	0.3	2	300	-	2	-3.1	0.2	2	473	-	2	-	-	-	-	-	-	-	-3.39	773
PL07-82Bx	3	0.01	10.69	64.97	818.00	-	-5.2	0.1	2	778	-	2	-3.0	0.7	2	301	-	1	-	-	-	-	-	-	-	-4.57	1079
PL07-105Bx	4	0.01	10.77	65.65	1296.00	-	-5.4	0.4	2	495	-	2	-2.4	0.3	2	402	-	2	-	-	-	-	-	-	-	-4.02	897
PL07-69Bx	5	0.01	10.77	64.61	545.00	-	-5.1	0.0	2	875	-	2	-2.1	2.1	2	310	-	2	-	-	-	-	-	-	-	-4.31	1185
PL07-111Bx	6	0.01	10.84	65.78	411.00	-	-5.3	0.2	2	355	-	2	-3.2	0.1	2	564	-	2	-	-	-	-	-	-	-	-4.01	919

Table 1. Thallium isotope and concentration data for USGS standard SCO-1 sediments, Black Sea, and Cariaco Basin. The map location for numbers for Cariaco Basin are the site locations that match with Figure 2. The number of replicate sediment digest analyses is identified by n.

	Mo (10^{14} moles)	$\delta^{98}\text{Mo}$ (‰)	Tl (10^6 moles)	$\epsilon^{205}\text{Tl}$
Initial marine reservoir	1.47	1.80	8.6	-6.0
	Mo Flux (10^7 moles/Ma)	$\delta^{98}\text{Mo}$ (‰)	Tl Flux (10^{10} moles/Ma)	$\epsilon^{205}\text{Tl}$
Riverine Input	29.9	0.78	112.5	-2.5
Hydrothermal Input	0.1	0.00	83.2	-2.0
Aerosol Input	-	-	24.5	-2.5
Volcanic Input	-	-	181	-2.0
Reducing sediment Input	-	-	83.2	0.0
Total Input	30	0.78	484.3	-1.8
Oxic Output	8.66	-1.46*	151.7	16†
Reducing Output	19.4	1.70*	-	-
Euxinic Output	1.94	^	-	-
Ocean alteration Output	-	-	332.7	-1.14†
Total Output	30	0.78	484.3	-1.8

Table 2. Initial parameters used in the Mo and Tl model (Anbar and Rouxel, 2007; Nielsen et al., 2017; Reinhard et al., 2013). Molybdenum fluxes are in 10^{14} mol/Ma and the reservoir size is 10^{14} mol. Dashes indicate phases that do not contribute significantly to the known isotopic mass balance for each element. The euxinic output for Mo (^) has been modeled to capture the seawater value with no fractionation. The Mo (*) and Tl (†) isotopic fractionation from seawater for each element.

Sample Name	Depth (m)	Latitude	Longitude	Average ²⁰⁵ Tl (€)	Data (2*std)	n	Average Tl (pg/g)	Data (2*std)	n
GeoTraces 40 °S Station 3									
21-186	4.838	-36.46	13.39	-6.0	-	1	11.7	-	1
19-184	22.6	-36.46	13.39	-5.8	-	1	-	-	-
17-181	47.427	-36.46	13.39	-5.8	-	1	11.1	-	1
9-178	97.164	-36.46	13.39	-6.1	-	1	-	-	-
15-175	195.896	-36.46	13.39	-6.0	-	1	-	-	-
13-172	395.392	-36.46	13.39	-5.8	-	1	12.1	-	1
11-170	594.034	-36.46	13.39	-6.1	-	1	-	-	-
9-169	989.446	-36.46	13.39	-5.9	-	1	10.8	-	1
7-168	1482.832	-36.46	13.39	-5.9	-	1	13.1	-	1
7-167	1974.651	-36.46	13.39	-5.9	-	1	11.9	-	1
5-166	2955.332	-36.46	13.39	-6.0	-	1	13.6	-	1
5-164	3930.994	-36.46	13.39	-6.2	0.0	2	11.4	-	1
Station Average				-6.0	0.27	12	12.0	1.9	12
GeoTraces 40 °S Station 6									
33-451	5.26	-39.99	0.92	-6.0	-	1	11.1	-	1
31-449	22.586	-39.99	0.92	-5.8	-	1	12.2	-	1
25-446	47.276	-39.99	0.92	-6.1	-	2	10.3	-	2
23-443	97.562	-39.99	0.92	-6.2	-	1	9.9	-	1
29-440	198.404	-39.99	0.92	-6.2	-	1	11.9	-	1
21-437	399.259	-39.99	0.92	-5.9	-	1	12.7	-	1
19-434	998.494	-39.99	0.92	-5.8	-	1	11.4	-	1
27-433	1498.258	-39.99	0.92	-5.9	0.1	2	12.2	-	2
13-432	1999.168	-39.99	0.92	-6.1	-	1	11.5	-	1
23-429	3999.614	-39.99	0.92	-6.1	-	1	13.0	-	1
11-428	4500.758	-39.99	0.92	-6.1	-	1	-	-	-
Station Average				-6.0	0.3	11	11.6	2.0	11
GeoTraces 40 °S Station 8									
35-903	29.55	-34.31	17.60	-6.2	-	1	9.2	-	1
33-901	49.465	-34.31	17.60	-6.1	0.4	2	10.3	-	1
31-897	98.873	-34.31	17.60	-6.1	0.3	2	9.5	-	2
7-893	198.181	-34.31	17.60	-6.1	0.3	2	10.2	-	1
23-889	400.494	-34.31	17.60	-6.1	0.1	2	11.4	-	1
9-884	719.388	-34.31	17.60	-6.2	0.0	2	9.2	-	1
Station Average				-6.1	0.1	6	10.0	1.7	6
GeoTraces 40 °S Station 11									
21-787	9.889	-39.29	7.65	-6.1	0.6	2	11.0	-	1
19-786	22.669	-39.29	7.65	-6.2	0.3	2	11.5	-	1
17-780	97.047	-39.29	7.65	-6.0	0.5	2	10.8	-	1
15-777	197.037	-39.29	7.65	-5.9	0.6	2	11.5	-	1
37-774	399.734	-39.29	7.65	-5.9	-	1	11.8	-	1
13-772	700.297	-39.29	7.65	-6.1	0.7	2	12.1	-	1
35-771	999.743	-39.29	7.65	-5.8	0.0	1	12.2	-	1
11-770	1501.777	-39.29	7.65	-5.8	0.2	2	10.9	-	1
9-769	1998.859	-39.29	7.65	-6.0	0.4	2	12.5	-	1
7-768	2998.972	-39.29	7.65	-5.9	-	1	11.8	-	1
5-766	5000.322	-39.29	7.65	-6.0	0.4	2	11.2	-	1
3-764	5259.82	-39.29	7.65	-5.9	-	1	11.9	-	1
Station Average				-6.0	0.2	12	11.8	1.1	12
SAFe Station									
1	0	30.00	-140.00	-6.0	-	1	-	-	-
2	0	30.00	-140.00	-5.8	-	1	12.2	-	1
3	0	30.00	-140.00	-6.0	-	1	10.2	-	1
4	0	30.00	-140.00	-6.1	-	1	12.5	-	1
5	0	30.00	-140.00	-5.9	-	1	-	-	-
6	0	30.00	-140.00	-5.8	-	1	14.0	-	1
7	0	30.00	-140.00	-6.2	-	1	11.9	-	1
8	0	30.00	-140.00	-6.3	-	1	-	-	-
Station Average				-6.0	0.3	8	12.2	2.7	8

Table 3. All open ocean seawater Tl concentration, isotope and location data. The number of replicate seawater split analyses is given (*n*).

Sample Name	Depth (m)	Latitude	Longitude	Average ²⁰⁵ Tl (‰)	Data (2*std)	<i>n</i>	Average Tl (pg/g)	Data (2*std)	<i>n</i>
<i>Cariaco Basin</i>									
Seawater 35	35	10.5	64.67	-5.4	-	1	12.1	-	1
Seawater 100	100	10.5	64.67	-5.9	-	1	12.1	-	1
Seawater 150	150	10.5	64.67	-5.2	0.4	2	12.3	-	1
Seawater 255	255	10.5	64.67	-	-	-	7.1	-	1
Seawater 300	300	10.5	64.67	-	-	-	5.3	-	1
Seawater 400	400	10.5	64.67	-	-	-	1.4	-	1
<i>Black Sea</i>									
Seawater 30	30	42.52	31.40	-2.2	0.3	4	7.2	1.3	3
Seawater 100	100	42.52	31.40	-0.8	0.3	2	2.2	0.0	2
Seawater 150	150	42.52	31.40	0.4	-	1	0.3	-	1

Table 4. Seawater data for euxinic basins analyzed in this study which includes concentration and isotope values. The number of replicate seawater split analyses is given (*n*).

Figure captions

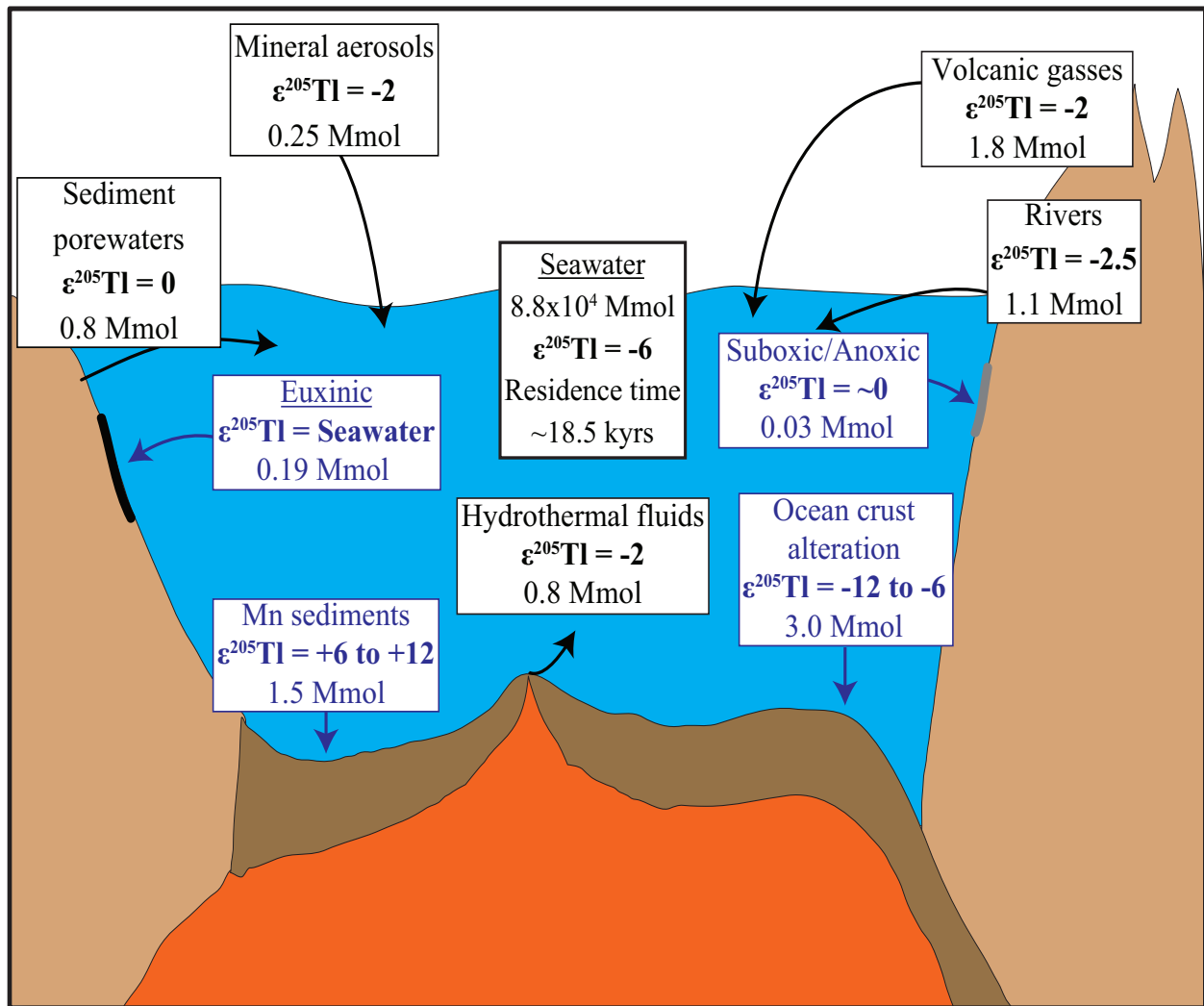


Figure 1. Updated mass balance modified from Nielsen et al. (2009; 2011b; 2017) and Baker et al. (2009) with new data from this study (headers underlined to indicate new data). Purple boxes represent the output fluxes which largely dictate the Tl isotope value of seawater. All fluxes are given in mega moles per year.

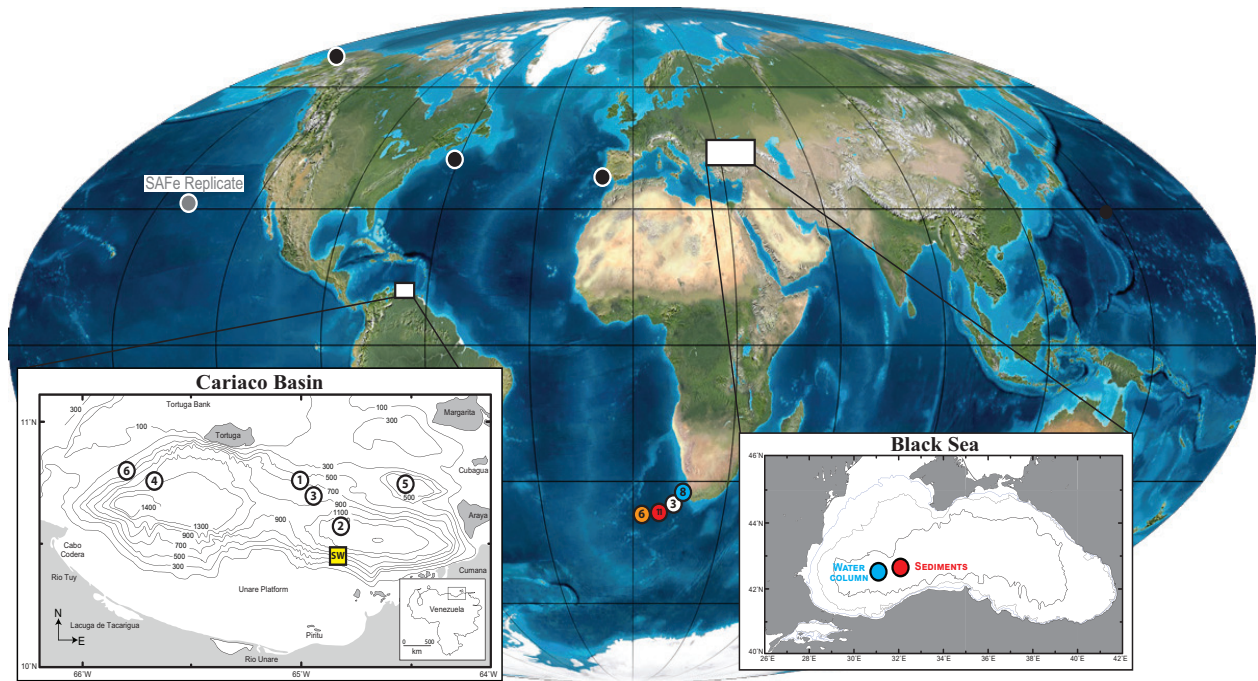


Figure 2. Map of modern seawater thallium isotope values. In the global ocean black circles represent previously reported $[Tl]$ and isotopes, blue circle, white circle, red circle, orange circle, and grey circle represent new seawater data presented here, and white boxes are modern euxinic basins for which we report $[Tl]$ and Tl isotopes from seawater and sediment samples. Cariaco Basin inset with numbered circles documenting core-top sediment sample locations and the square representing the location of the seawater samples. Inset of the Black Sea with the location of seawater samples and sediment samples.

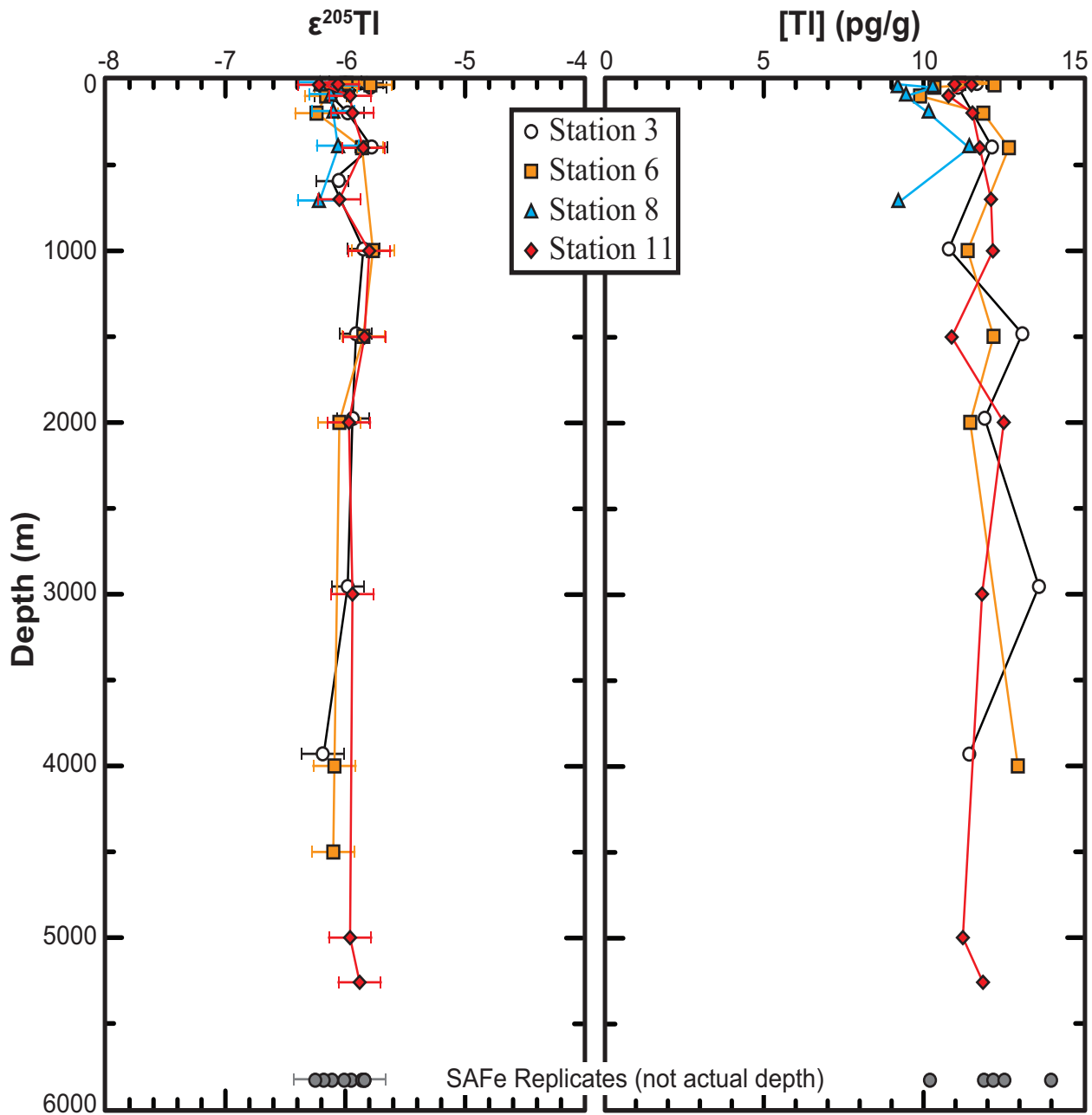


Figure 3. Vertical and spatial seawater transect from UK GEOTRACES 40° S cruise in the southern most Atlantic Ocean (Fig. 1). Error bars are 2σ for separate replicate analyses.

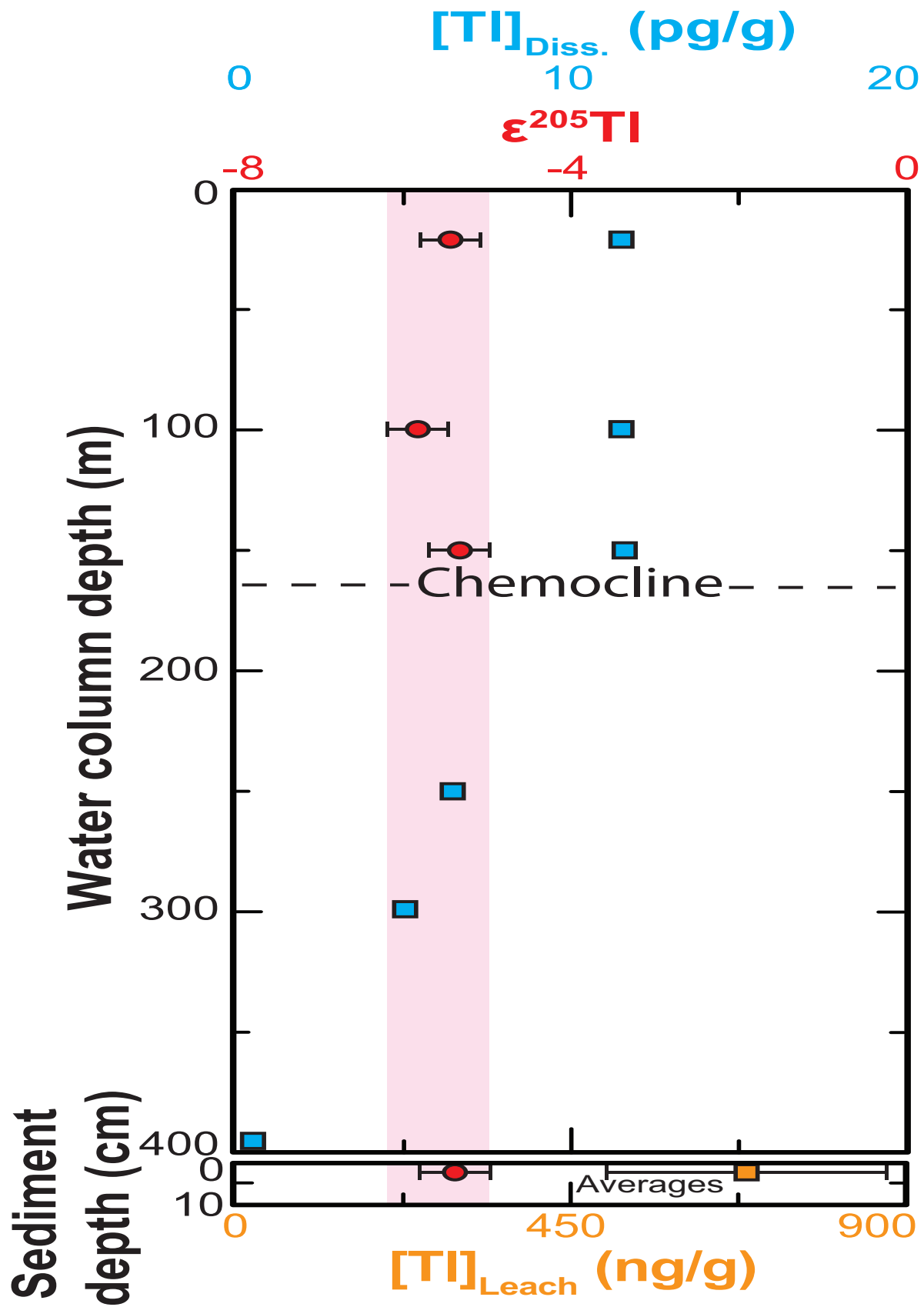


Figure 4. Cariaco seawater depth transect of $\epsilon^{205}\text{Tl}$ and $[\text{Tl}]$ and average core top sediment values (excluding one outlier). The sulfide concentrations increase at ~ 160 m marked by the dashed line indicating typical depth of the chemocline. Error bars are 2σ for separate replicate analysis. Vertical pink bar represents the entire range of Cariaco seawater of $\epsilon^{205}\text{Tl}$ seawater values which encompasses the average $\epsilon^{205}\text{Tl}$ sediment value. Note the $[\text{Tl}]$ and $\epsilon^{205}\text{Tl}$ for seawater (upper panel) is the dissolved concentration and sediment $[\text{Tl}]$ and $\epsilon^{205}\text{Tl}$ values are from the leached fraction.

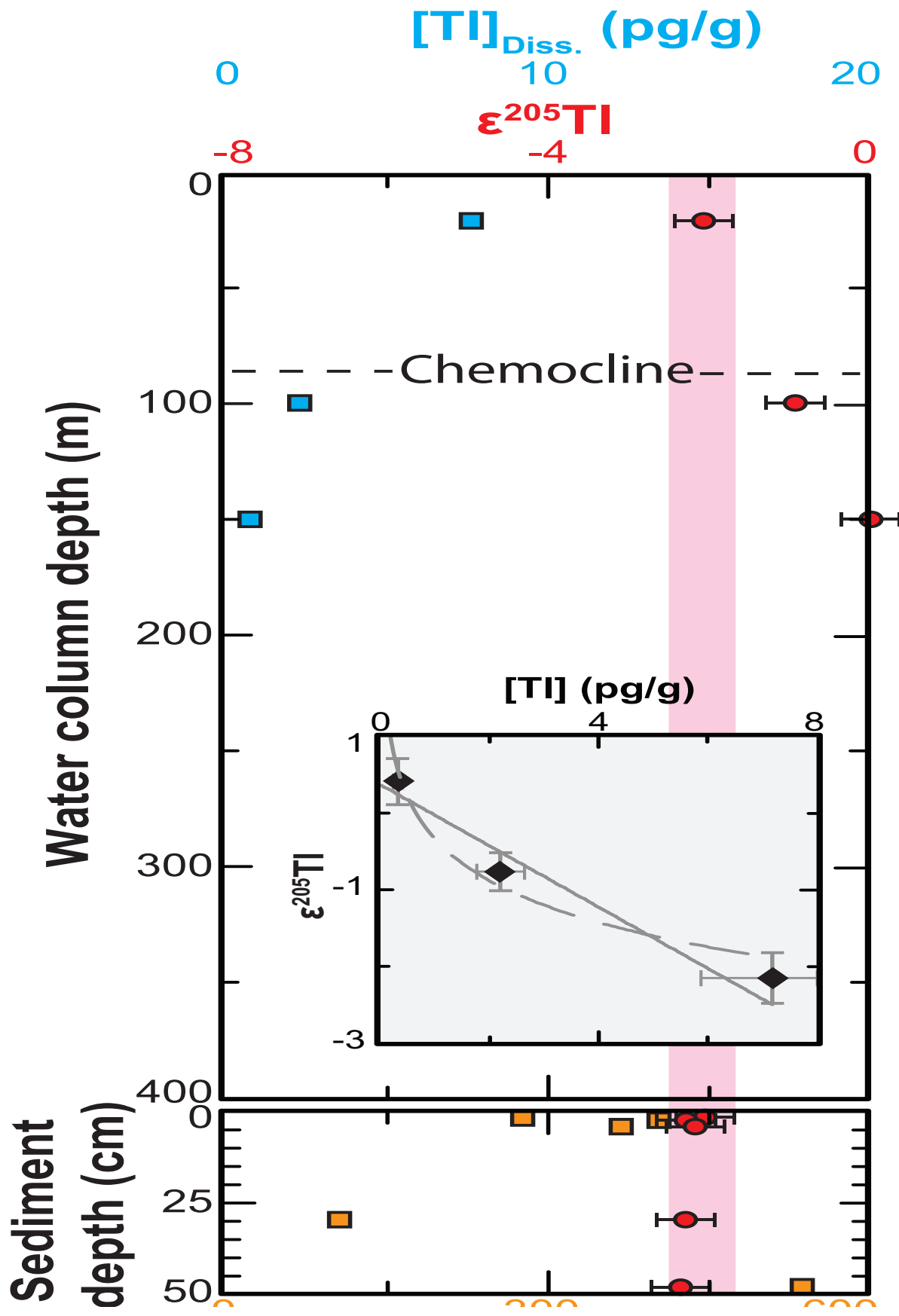


Figure 5. Black Sea depth transect of seawater samples for Tl isotopes and concentration. Chemocline is at ~90 m at this site. Error bars are 2σ for separate replicate analysis. Inset figure is the calculated fractionation with closed system Rayleigh distillation (dashed line) and open system steady state fractionation (solid line). Vertical pink bar represents the entire range of Black Sea $\epsilon^{205}\text{Tl}$ seawater values which also encompasses the range $\epsilon^{205}\text{Tl}$ sediment value. Note the $[\text{Tl}]$ and $\epsilon^{205}\text{Tl}$ for seawater (upper panel) is the dissolved concentration and sediment $[\text{Tl}]$ and $\epsilon^{205}\text{Tl}$ values are from the leached fraction.

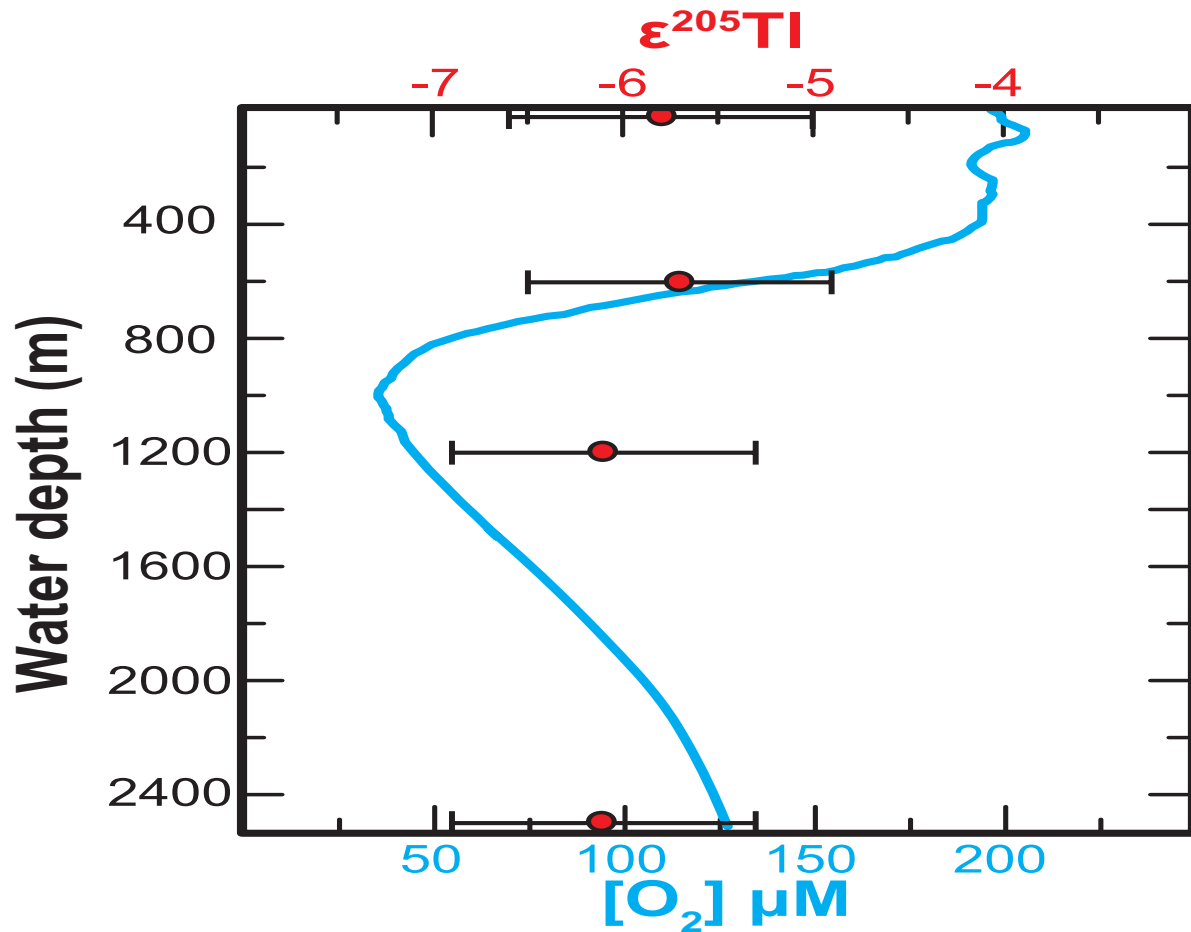


Figure 6. Depth transect of seawater Tl isotopes and oxygen content from a Pacific oxygen minimum zone locality.

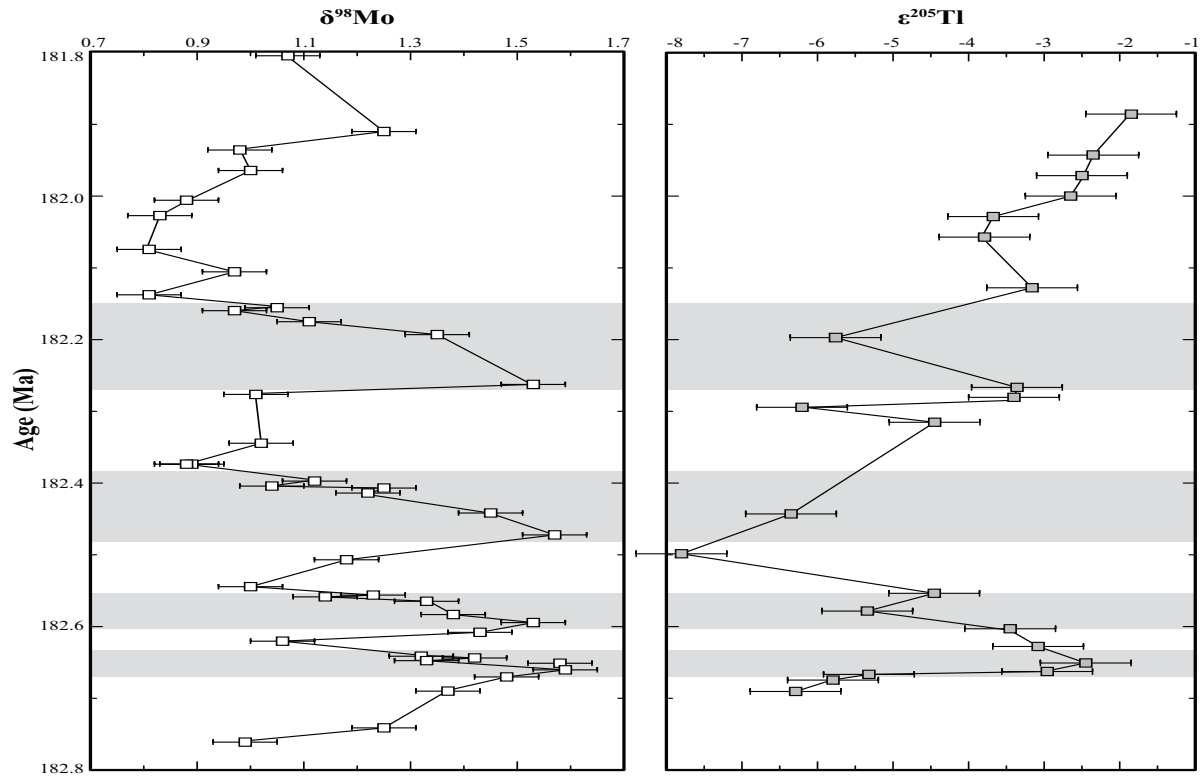


Figure 7. Yorkshire isotope values for thallium and molybdenum during the Toarcian Oceanic Anoxic Event which are replotted from Pearce et al. (2008) and Nielsen et al. (2011b). These data show the possible antithetic relationship of these two isotopic systems.

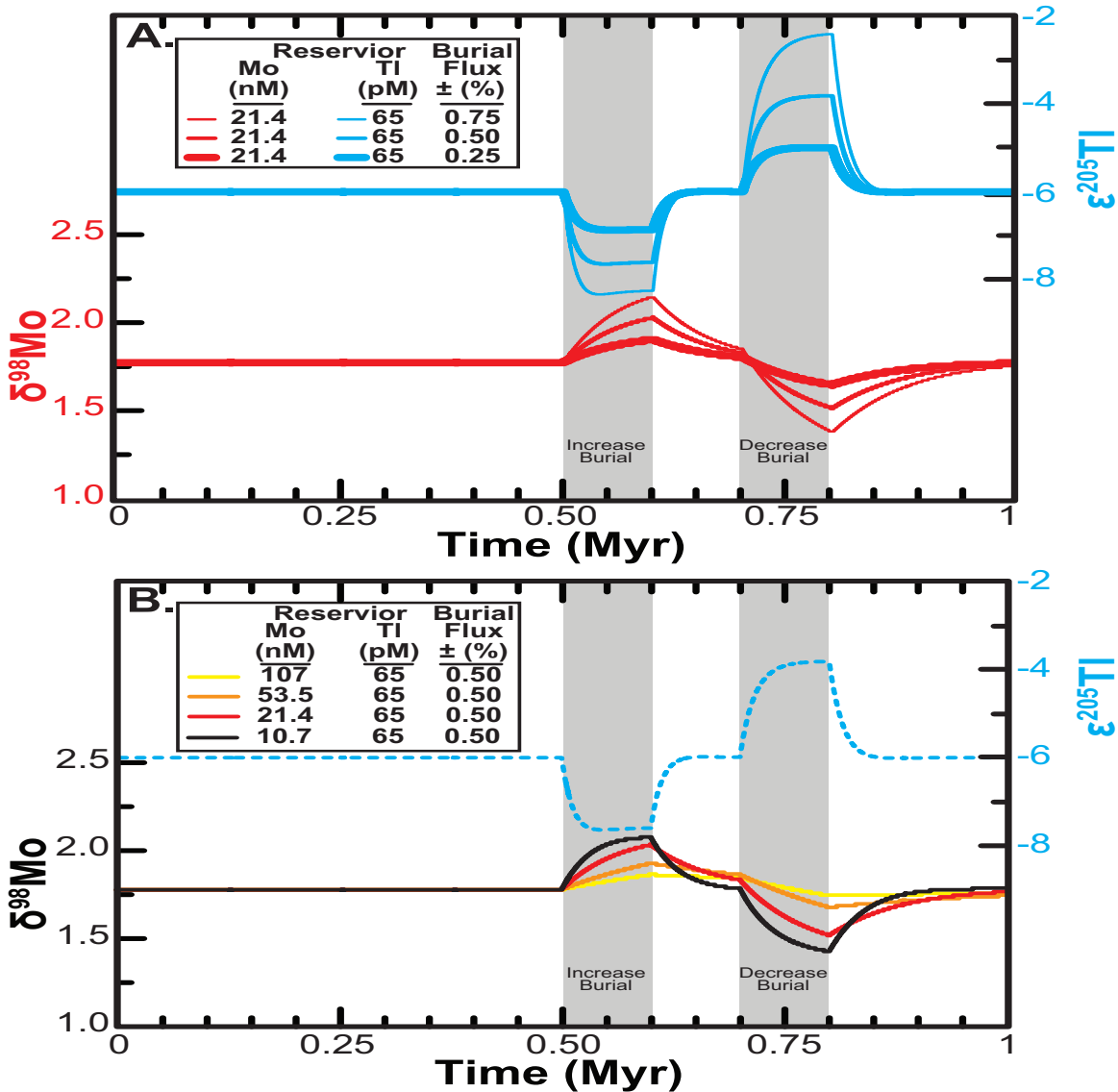


Figure 8. Modeling variation in the global ferro-manganese oxide burial and the antithetic relationship between thallium and molybdenum isotopes. This model depicts how variations in oxide burial can control Mo and Tl isotopes in opposite directions. For all runs, the first 0.5 Ma was held at steady state with an increased burial for 100 thousand years, between 0.5 and 0.6 Ma, values then returned to background for 100 thousand years, followed by a decrease in oxide burial for 100 thousand years and lastly burial fluxes were returned to baseline values. Part A. varies oxide burial for each run using modern starting values for Mn-oxide burial, concentration for Tl and 20% modern for Mo (21.4 nM). Part B. varies the starting concentration for Mo in each run and keeps for all runs Mn-oxide fluxes the same at 50% modern values. Burial between 1 and 1.25 Ma and starting values returning at 1.25 Ma. For starting values see Table 1.